

Structural, electronic and topological properties of 3D TmBi compound

M. Ragragui^{1,2}, L. B. Drissi^{1,2,3,4,*}, S. Lounis^{4,5}, E. H. Saidi^{1,2,3}

1-LPHE, Modeling & Simulations, Faculty of Science,

*Mohammed V University in Rabat, Morocco**

2- CPM, Centre of Physics and Mathematics,

Faculty of Science, Mohammed V University in Rabat, Morocco

3-College of Physical and Chemical Sciences,

Hassan II Academy of Sciences and Technology,

Km 4, Avenue Mohammed VI, Rabat, Morocco

4-Peter Grünberg Institut and Institute for Advanced Simulation,

Forschungszentrum Jülich & JARA, Germany and

5-Faculty of Physics, University of Duisburg-Essen, 47053 Duisburg, Germany

Abstract

Using density functional theory based methods we report the structural, electronic and topological properties of the FCC crystal compound TmBi. This material is found to be dynamically stable and shows a non magnetic semimetallic character. By tuning the spin-orbit coupling, we observe a significant change in the band structure, and the occurrence of band inversion along $\Gamma - X$ direction. The parity product at time-reversal invariant momentum points and the Wannier charge center calculations provide a topological index $Z_2 = 1$ on the $k_j = 0$ plane (with $j = 1, 2$ and 3) revealing the non trivial topological character of TmBi. The existence of topologically protected surface states of TmBi through the observation of a Dirac cones at \bar{X} point confirm our finding. The present work could inspire platforms for exploring novel topological states within the family of rare-earth monobismuthides.

Keywords: Rare earth compounds; electronic structure; phonon calculations; topological index; Dirac cone surface states.

***Corresponding author:** Lalla Btissam Drissi, E-mail addresses: lalla-btissam.drissi@fsr.um5.ac.ma, l.drissi@fz-juelich.de

I. INTRODUCTION

Topological electronic materials, such as topological insulators (TI) and topological semimetals (TS) with time reversal (TR) symmetry, are quantum states of matter exhibiting novel linear responses in the bulk and protected surface states [1–4]. A much richer bulk-boundary correspondence where gapless states live in boundary corners and hinges of bulk has also attracted a big deal of attention in the few recent years [5–9]. Interestingly, the classification of topological phases depends on two main ingredients: (i) the dimensionality of the bulk material and (ii) discrete symmetries protecting boundary states. Refs [10–12] derived first ingredients to capture distinctive features of topological phases of matter. Other approaches involving the quantized Wannier center [13, 14], the signature index [15] and the Berry phase [16] have also been developed.

In conventional topological insulators, the band inversion in the bulk spectrum, mainly attributed to spin-orbit interaction, is crucial to distinguish between topological non trivial and topological trivial phases [17–19]. Furthermore, the presence of both time reversal and inversion symmetry in these systems allows the determination of a \mathbb{Z}_2 topological invariant to confirm the topological non trivial character of the bulk material [20–22]. TIs with broken rotation symmetry switch to Weyl semimetals [23]. However, breaking TR symmetry converts some Dirac semimetals to Weyl semimetals having both zero gap energy at their Fermi level [24]. The energy-momentum dispersion is linear in all momentum directions in Dirac and Weyl semimetals [25], and the corresponding Fermi surfaces are formed by points or lines in topological nodal semimetals [26–28]. Topological boundary modes emerging as chiral Fermi arcs have been observed for Cd_3As_2 and Na_3Bi using ARPES measurements [29, 30]. TaAs and WTe_2 materials are Type-I Weyl semimetals characterized with standard point-like Fermi surfaces [31, 32].

Rare-earth (RE) monpnictide /monoantimonides/monobismuthides are binary compounds hosting extremely large magnetoresistance [33–35]. Rare-earth monpnictides, including LaX ($X = \text{N, P, As, Sb, Bi}$) and DyY ($Y = \text{P, As, Sb}$) compounds exhibit exotic electronic surface states and different topological character [37–40]. A Dirac-like feature is observed within specific photon energy range in rare-earth monoantimonides YSb , CeSb , and GdSb , while most RESb ($\text{RE} = \text{Y, Ce, Gd, Dy, Ho, Tm, Lu}$) compounds are topologically trivial [41, 42]. ARPES measurements demonstrate possible Dirac fermion in the strongly correlated cerium monpnictides CeSb , and the absence of band inversion in both the three dimensional band structure of LaSb and CeSb [43–45].

Despite the increasing interests in RESb/REBi systems and their homologues, theoretical studies of topological aspects of some rare-earth monobismuthides are still missing. In this paper, we investigate for the first time to our knowledge, the face-centred cubic TmBi system with and without spin orbit coupling (SOC). We first examine its structural stability using phonon analysis. Then, we show the presence of bulk band inversion and the existence of surface Dirac cones using different techniques of topological theory.

The paper is organised as follows; the computational method is detailed in section 2. We report and discuss the obtained results in Section 3. We end with a conclusion commenting our findings.

II. COMPUTATIONAL DETAILS

In this article, we employ first principles calculations based on Density Functional Theory (DFT), with the Projected Augmented Wave (PAW) method implemented in the Quantum espresso (QE) package [46]. The generalized gradient approximation (GGA) is used for the exchange correlation energy function [47]. To ensure convergence of our calculations, we employ a plane-wave basis up to 480 eV and $12 \times 12 \times 12$ Γ -centered K mesh, so that the total energy converges to 1 meV per cell. SOC is included in the self-consistent electronic structure calculations, and f-electrons have been treated as core electrons. Since GGA function is known to exaggerate the band inversion features, we fit the GGA-DFT-band structure to a tight-binding Hamiltonian using the maximally localized Wannier function method [48, 49] with Tm d-orbitals and Bi p-orbitals. Based on the obtained data, we calculate the hybrid Wannier charge centers(WCCs) [50]. These calculations are performed to establish the topological character using the wanniertools code [51] using an arbitrary line in half of Brillouin Zone (BZ) by calculating the number of crossings of WCCs mod2. The surface spectral functions are also calculated and given. For the phonon dispersion spectrum, a $4 \times 4 \times 4$ supercell was used.

III. RESULTS AND DISCUSSION

In this section, we investigate the topological properties of Thulium monobismuthide using systematic first-principles studies. Optimized lattice parameters and phonon dispersion spectra with and without SOC are reported. The presence of bulk band inversion and the existence of surface Dirac cones are shown.

A. Lattice stability of TmBi

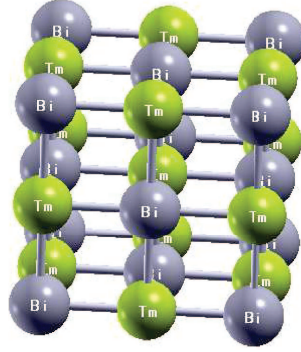


FIG. 1: The FCC unit cells of TmBi; the grey balls correspond to Bi atoms and the yellow ones present the Tm atoms.

TmBi crystallizes into a face-centred cubic structure belonging to the space group $Fm\bar{3}m$ (No. 225), in which the Tm atom is positioned at $(0.5, 0.5, 0.5)$ and Bi atom at $(0, 0, 0)$, as shown in Fig.1. The optimization of the TmBi structure deals with a lattice parameter $a=6.255 \text{ \AA}$ used later for the phonons and band structure calculations.

In the absence of any theoretical and experimental study of lattice dynamics of TmBi, we investigate the phonon dispersion spectrum with and without spin-orbit interaction. The shapes of the corresponding curves, plotted in Figs 2, are rather similar with a small gap observed between the acoustic and optical branches in the absence of spin orbit coupling. One can also notice that the obtained range of phonon frequency is from 0 to 4 THz (120 cm^{-1}). Furthermore, no negative frequencies are observed for TmBi in the Brillouin zone, which indicates a perfect kinetic stability of this structure and confirms its thermodynamic stability.

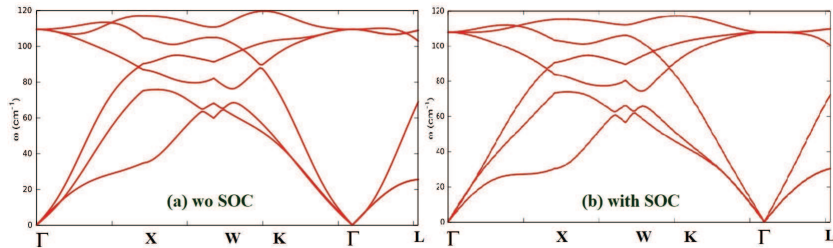


FIG. 2: TmBi's Phonon dispersion spectra: a) without SOC, b) with SOC.

B. Electronic properties

From the partial density of states (PDOS) curves displayed in Fig.3, we have analyzed the elementary contribution of all atomic orbitals. **In the absence of SOC**, it is shown in Fig.3-a that near the Fermi level, the valence band (VB) is a mixture of Bi(2p)-orbitals and small contribution of Tm(5d)-orbitals. On the other hand, the conduction band (CB) mainly consists of Tm(5d) and (2s)-states with a small contribution of Bi(2p)-orbitals. Strong hybridization between Tm- and Bi-orbitals is observed in the valence bands far from Fermi level at nearly -1.8 eV. One deduces that TmBi is a non magnetic semi-metal compound in good agreement with other topological semimetal materials like PrBi [52], LaBi [33] and LaSb [35].

When SOC the spin-orbit interaction is considered, the partial density of states in Fig.3-b reveals that the Bi p-orbitals splits degenerate into $\mathbf{p}_{\frac{3}{2}}$ - and $\mathbf{p}_{\frac{1}{2}}$ - orbitals. More precisely, the $\mathbf{p}_{\frac{1}{2}}$ - Bi orbital goes into the valence band around -2.5 eV and the $\mathbf{p}_{\frac{3}{2}}$ - Bi orbitals contribute near the Fermi level and in the valence band around -1.5 eV. Furthermore, the Tm d-orbitals split into $e_g(\mathbf{d}_{z^2}, \mathbf{d}_{x^2-y^2})$ and $t_{2g}(\mathbf{d}_{xz}, \mathbf{d}_{yz}, \mathbf{d}_{xy})$, where the spin orbit interaction further splits t_{2g} into doubly degenerate and non-degenerate orbitals. Thus, near the Fermi energy, the bands are dominated by contributions from p-states of Bi and Tm-d states, whereas other states are mostly unfilled with small contribution. The present result is comparable with PrBi material [36].

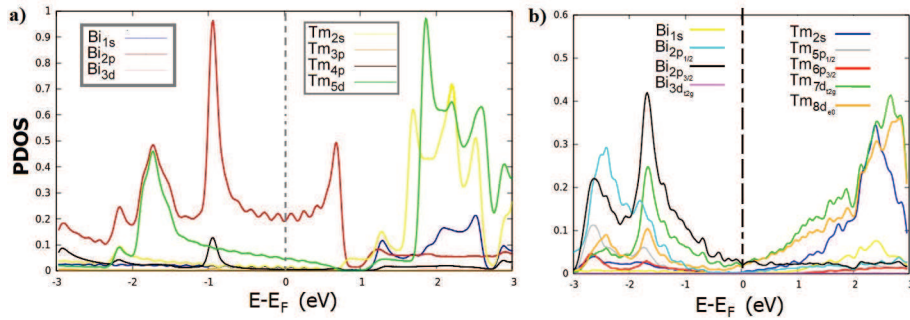


FIG. 3: Partial density of states (pdos) for a) non-spin-orbit calculation and b) with SOC.

The energy band structures of TmBi along high symmetry lines using GGA and GGA+SOC are plotted in Fig.4. In the absence of SOC, there are one electron-like band at the X-point and three hole-like bands at the Γ -point that cross the Fermi level overlapping together to create a continuous gap along the whole Brillouin zone in each k-point. Furthermore, a direct energy gap occurs in two locations: (i) at 0.5 eV below Fermi level along Γ -X direction and (ii) in the

conduction band at Γ point.

When the SOC effect is included into the calculations, a significant change of the degeneracy of bands-states in the whole Brillouin zone is depicted in the band structure near E_F as shown in Fig.4-b. Indeed, the whole band shifts toward lower binding energy and only a small part of the band persists above E_F at Γ -point. In turn, the two highest energy bands below Fermi level become noticeably separated from each other along Γ -X path creating a small gap around 43 meV. The gap observed at the anticross point increases to 144 meV at the X-point. Our result within SOC creating an anti-cross is also observed for LaX (X=As,Sb,Bi) [28],[37]-[39] and reported in earlier calculations for YsSb [42] and dysperium monopnictides [40]. Furthermore, our calculated band structures with and without SOC, concorde well with the ones of monobismithudes materials, like LaBi, LaSb, and PrBi [45] since the overall dispersion is very similar, with four bands crossing the Fermi level, more precisely: threefold degenerate hole-like bands pinned at about 0.5 eV above E_F at the Γ -point and one elongated electron band close to the X-point at the border of the Brillouin zone (BZ). It is worth noting that we find the same result using LDA and LDA+SOC calculations as listed in Table-I. One can see that LDA slightly increases the gaps with respect to GGA. This result is a first signature of the topological character of our compound as confirmed in the the following discussion.

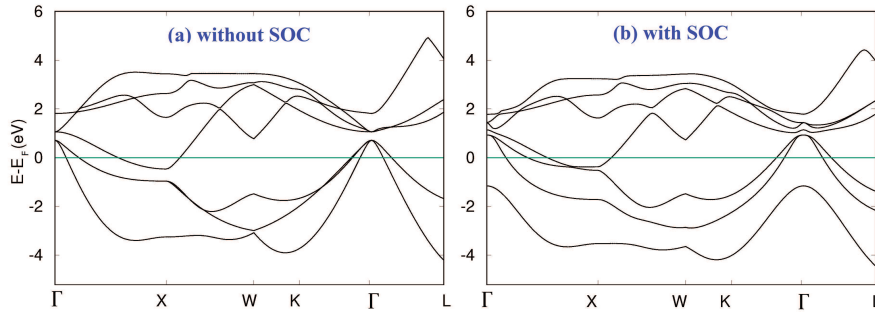


FIG. 4: Band structure of TmBi (a) without spin orbit coupling , b) with spin orbit coupling.

It is clear from Figs.5 that there is no band inversion at Γ -point. In contrast, the conduction band and valence band give rise to band inversion along Γ -X direction, and the orbital character of band changes near the X-point which predict the topological character of TmBi as reported in other materials such as GdBi and PrBi [45]. TmBi exhibits band inversion between the Tm-5d and Bi-2p states similar to PrBi [45]. Fig.5 shows the calculated GGA+SOC projected bulk band structure in the entire Brillouin zone for TmBi. The bands near the Fermi level mainly come from

TABLE I: The energy gap near and at X point with both GGA and LDA calculations.

Gap energy (eV)	Near X point	At X point
GGA	-	0.498
GGA+SOC	0.043	0.144
LDA	-	0.4564
LDA+SOC	0.053	0.2

Tm (5d)-orbitals and Bi (2p)-orbitals, as indicated by different colors in Fig.3 and discussed in the PDOS analysis. Near the X-point, the Tm (5d)-band indicated by red color crosses the green band of Bi (2p), creating an inverted small band gap and resulting in non-trivial band topology. This band inversion is due to the odd parity of Bi-2p orbitals and even parity of Tm-5d orbitals. This d-p band inversion was recently reported for LaBi and Prbi [39, 45], but such band inversion is absent in LaSb and CeSb [43].

In what follows, we examine this topological characteristic according to the topological theory.

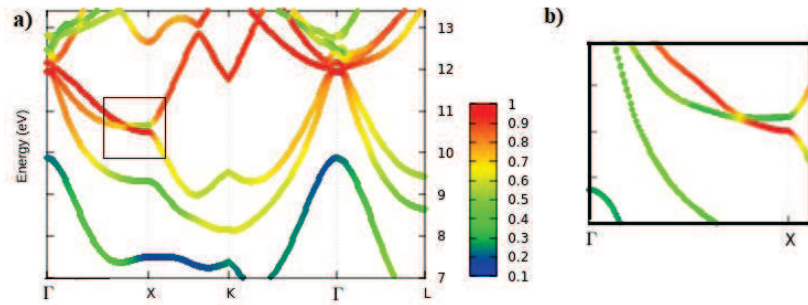


FIG. 5: Calculated bulk band structure in (a) the entire Brillouin zone and (b) along the $\Gamma - X$ direction for TmBi, showing the predicted bulk band inversion between Tm 5d(red) and Bi 2p(green) bands near the X point.

C. Topological index and surface states

Recall that our system preserves both time-reversal symmetry and inversion symmetry. It follows that the \mathbb{Z}_2 topological invariant for the 3D bulk TmBi that characterizes a topological insulator can be calculated directly by the parity product of fully occupied valence bands at eight

time-reversal invariant momentum points (TRIM) [2]. The \mathbb{Z}_2 topological index, referred to as ν_0 , is deduced from the following formula

$$(-1)^{\nu_0} = \prod_{i=1}^8 \prod_{n=1}^N \delta_n(\Gamma_i) \quad (1)$$

where δ_n is the parity product of the valence bands at the n -th TRIM point, the products are over TRIM-point and the Kramers pairs of occupied bands, respectively.

In this context, our analysis of bands structure of TmBi shown in Fig.4 reveals that there is a gap between conduction and valence bands at each k -point. Within GGA+SOC, we find that TmBi possesses a non trivial topological index $\mathbb{Z}_2 = 1$. The band parity of the eight TRIM points, namely one Γ -point, three X-points and four L-points, are listed in Table-II.

TABLE II: Band parity of 8 TRIM points along BZ of TmBi

	TmBi
TRIM Points	δ_n
1 Γ	+
3X	-
4L	+

The \mathbb{Z}_2 -index is also obtained by tracing the evolution of Wannier charge centers of fully occupied Bloch bands for six time-reversal invariant momentum planes, namely ($k_j = 0$ and π , with $j = 1, 2$ and 3). As clearly shown in Fig.6, the even number of crossings between the reference line and evolution lines indicates that $\mathbb{Z}_2 = 0$ for $k_j = \pi$ -plane, while the reference line has odd number of intersections with the evolution lines confirming that $\mathbb{Z}_2 = 1$ for $k_j = 0$ -plane. Consequently, the \mathbb{Z}_2 index for TmBi is 1 at (000)-plane which concordes well with our previous results reported in band structure calculations, predicting the existence of nontrivial surface states in TmBi. It is worth noting that similar nontrivial \mathbb{Z}_2 topological index, and hence topological surface states with bulk band inversion are predicted, using the same numerical calculations, for REBi family (with RE ranging from Ce to Gd), for some rare-earth monobismuthides with partially filled f shell, including SmSb, GdSb, DyBi, and YbBi, and for dysprosium monopnictides compounds, namely DyP, DyAs and DySb [39, 40, 43, 45].

Recall that in the FCC structure rock salt there is three X-points, and one Γ -point. To confirm the topological non-trivial electronic structure at the [111] surface of TmBi, we firstly perform

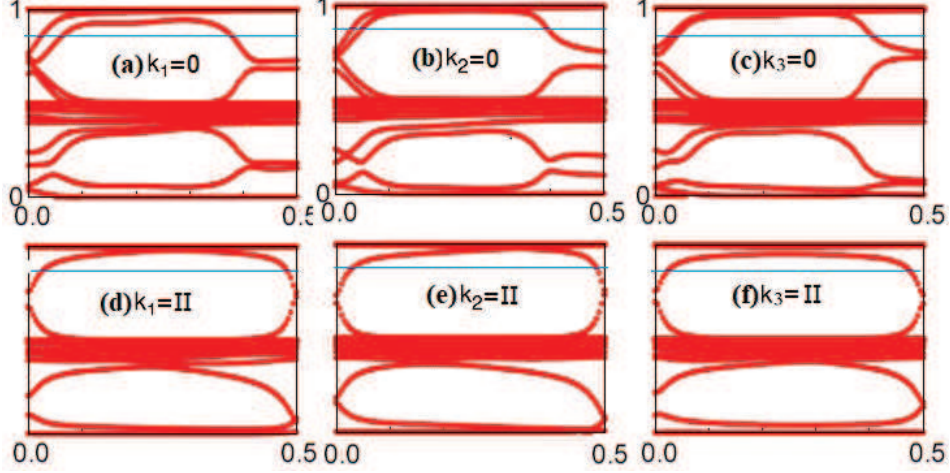


FIG. 6: Evolution of the Wannier centers θ as a function of k_j for the time-reversal invariant planes (a,b,c) $k_j = 0$, and (d,e,f) $k_j = \pi$ of the bulk Brillouin zone. A reference line (Blue) is used to determine the Z_2 topological invariant of the k_3 -plane.

surface state calculations along $\Gamma - \bar{X} - M$ direction by employing the Green's function approach based on a tight-binding model Hamiltonian derived from our first principles calculations. The result along $\Gamma - \bar{X} - K$ and along $\Gamma - \bar{X} - \Gamma$ is depicted in Fig.7 for more visibility. Our calculations reveal that no single Dirac cone appears at Γ , while a Dirac cone surface state is clear observed at \bar{X} -point in good agreement with the projection of band inversion. Therefore, one has an odd number of Dirac cones on the [111] surface. This finding concordes well with LaBi, CeSb, CeBi, PrBi topological semimetals and DyY compounds with (Y=P,As), where the presence of topological surface states is prominent [37, 39, 43, 45]. In contrast, unusual topological surface states with high anisotropic Dirac-like cone are observed in DySb rock salt structure and half-Heusler material LnPtBi [45, 53], while only bulk states are visible in YbSb compound.

It follows that TmBi material can provide an excellent platform for exploring topological surface states in 3D semimetals which are strongly required for applications in spintronics and for electronic devices. Furthermore, it can exhibit high carrier mobility as well as unusual extreme magnetoresistance (XMR) property like some rare-earth monpnictides and monobismithudes previously cited. Therefore, it may help to investigate topologically trivial XMR material and discovery of a relationship between topology and the XMR effect which is still not established.

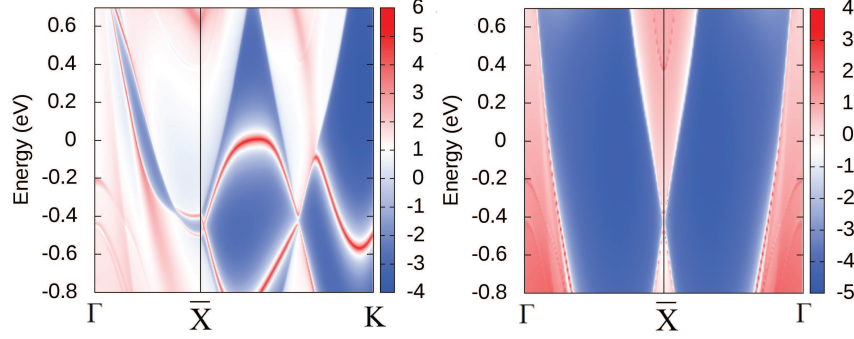


FIG. 7: Calculated Topological surface states of TmBi along $\Gamma - \bar{X} - K$ (a) and along $\Gamma - \bar{X} - \Gamma$ (b).

IV. CONCLUSION

Based on density functional theory calculations, the phonon dispersion spectrum of TmBi compound confirms its structural stability. The bulk electronic structure of these rock salt-type crystal in the form is nonmagnetic and semi-metallic. We have examined the low-energy bands near X point to show significant band inversion due to SOC interactions. To confirm the topological character of TmBi from the bulk we have determined \mathbb{Z}_2 -invariant for TmBi by two methods, namely the parity product at TRIM points and the Wannier charge center calculations. Dirac cone surface states connecting the conduction and valence band, have also been observed. The present finding on a pristine surface of a strong topological material could inspire new strategies to design new materials with novel functionalities and searching for exotic topological non trivial properties.

Acknowledgment 1 *The authors would like to acknowledge the "Académie Hassan II des Sciences et Techniques"-Morocco for its financial support. L. B. Drissi acknowledges the Alexander von Humboldt Foundation for financial support via the George Forster Research Fellowship for experienced scientists (Ref 3.4 - MAR - 1202992).*

-
- [1] Bernevig, B. A., Hughes, T. L. & Zhang, S. C. Quantum spin hall effect and topological phase transition in HgTe quantum wells. *Science* **314**, 1757 (2006).
- [2] Fu, L., and C. L. Kane. Topological insulators with inversion symmetry. *Phys. Rev. B* **76**, 045302 (2007).

- [3] Hsieh, D. et al. A topological Dirac insulator in a quantum spin Hall phase. *Nature* 452, 970–974 (2008).
- [4] Moore, J. E. & Balents, L. Topological invariants of time-reversal-invariant band structures. *Phys. Rev. B* **75**, 121306(R) (2007).
- [5] N. Bultinck, B. A. Bernevig, and M. P. Zaletel, Three dimensional superconductors with hybrid higher-order topology, *Phys. Rev. B* 99, 125149 (2019).
- [6] F. Schindler, Z. Wang, M. G. Vergniory, A. M. Cook, A. Murani, S. Sengupta, A. Y. Kasumov, R. Deblock, S. Jeon, I. Drozdov, H. Bouchiat, S. Gueron, A. Yazdani, B. A. Bernevig, and T. Neupert, Higher-order topology in bismuth, *Nat. Phys.* 14, 918 (2018).
- [7] L.B. Drissi, E.H. Saidi, Dirac zero Modes in Hyperdiamond Model, *Phys. Rev. D* 84, 014509 (2011)
- [8] V. Dwivedi, C. Hickey, T. Eschmann, and S. Trebst, Majorana corner modes in a second-order Kitaev spin liquid, *Phys. Rev. B* 98, 054432 (2018).
- [9] L. B. Drissi, E. H. Saidi, Domain Walls in Topological Tri-hinge Matter, *European Physical Journal Plus* 136, (68) (2021).
- [10] W. A. Benalcazar, B. A. Bernevig, and T. L. Hughes, Quantized electric multipole insulators, *Science* 357, 61 (2017).
- [11] F. K. Kunst, G. van Miert, and E. J. Bergholtz, Lattice models with exactly solvable topological hinge and corner states, *Phys. Rev. B* 97, 241405 (2018).
- [12] F. Schindler, A. M. Cook, M. G. Vergniory, Z. Wang, S. S. Parkin, B. A. Bernevig, and T. Neupert, Higher order topological insulators, *Science advances* 4, eaat0346 (2018).
- [13] F. K. Kunst, G. Miert, and E. J. Bergholtz. Lattice models with exactly solvable topological hinge and corner states. *Phys. Rev. B* 97, 241405(R) (2018)
- [14] M. Ezawa, *Phys. Rev. Lett.* 120, 026801 (2018).
- [15] L.B. Drissi, E.H. Saidi, A Signature Index for Third Order Topological Insulator. *J. Conden. Matter Phys.* 5; 32(36), 365704 (2020).
- [16] Hiromu Araki, Tomonari Mizoguchi, Yasuhiro Hatsugai, ZQ Berry Phase for Higher-Order Symmetry-Protected Topological Phases, *Phys. Rev. Research* 2, 012009 (2020).
- [17] A. Altland and M. R. Zirnbauer, *Phys. Rev. B* 55, 1142 (1997).
- [18] Fu, L., Kane, C. L., & Mele, E. J. Topological insulators in three dimensions. *Phys. Rev. Lett.* **98**, 106803 (2007).
- [19] Qi, X. L. & Zhang, S. C. Topological insulators and superconductors. *Rev. Mod. Phys.* **83**, 1057 (2011).

- [20] Roy, R. \mathbb{Z}_2 classification of quantum spin hall systems: an approach using time-reversal invariance. *Phys. Rev. B* 79, 195321 (2009).
- [21] Hasan, M. Z. & Kane, C. L. Colloquium: topological insulators. *Rev. Mod. Phys.* **82**, 3045 (2010).
- [22] L. B. Drissi, E.H. Saidi, M. Bousmina, Electronic properties and hidden symmetries of graphene, *Nucl.Phys.B*, **829**, Issue 3, (2010).
- [23] Lv, B. Q. et al. Experimental discovery of Weyl semimetal TaAs. *Phys. Rev. X* 5, 031013 (2015).
- [24] Wan, X., Turner, A. M., Vishwanath, A. Savrasov, S. Y. Topological semimetal and Fermi-arc surface states in the electronic structure of pyrochlore iridates. *Phys. Rev. B* 83, 205101 (2011).
- [25] M. Neupane, S. Xu, R. Sankar, N. Alidoust, G. Bian, C. Liu, I. Belopolski, T. Chang, H. Jeng, H. Lin, A. Bansil, F. Chou, and M. Z. Hasan. Observation of a three-dimensional topological Dirac semimetal phase in high-mobility Cd_3As_2 . *Nat Commun* 5, 3786 (2014).
- [26] Young, S. M. et al. Dirac semimetal in three dimensions. *Phys. Rev. Lett.* 108 (2012).
- [27] Burkov, A. A. & Balents, L. Weyl semimetal in a topological insulator multilayer. *Phys. Rev. Lett.* 107, 127205 (2011).
- [28] Feng, Baojie, et al. Experimental observation of node-line-like surface states in LaBi. *Physical Review B* 97.15 155153 (2018).
- [29] S. Borisenko, Q. Gibson, D. Evtushinsky, V. Zabolotnyy, B. Buchner, and R. J. Cava., Experimental Realization of a Three-Dimensional Dirac Semimetal. *Phys. Rev. Lett.* 113, 027603 (2014).
- [30] Z. K. Liu, B. Zhou, Y. Zhang, Z. J. Wang, H. M. Weng, D. Prabhakaran, S.-K. Mo, et al., Discovery of a Three-Dimensional Topological Dirac Semimetal, Na_3Bi , *Science* 343, 6173, (2014) 864-867.
- [31] A. A. Soluyanov, D. Gresch, Z. Wang, Q. Wu, M. Troyer, X. Dai, and B. A. Bernevig. Type-II Weyl Semimetals. *Nature* 527, 495 ,1507.01603 (2015).
- [32] Y. Wu, D. Mou, N. H. Jo, K. Sun, L. Huang, S. L. Bud'ko, P. C. Can eld, and A. Kaminski. Observation of Fermi arcs in the type-II Weyl semimetal candidate WTe_2 . *Phys. Rev. B* 94, 121113 (2016).
- [33] Guo, P.-J., Yang, H.-C., Zhang, B.-J., Liu, K. and Lu, Z.-Y. Charge compensation in extremely large magnetoresistance materials LaSb and LaBi revealed by first-principles calculations. *Phys. Rev. B* 93, 235142 (2016).
- [34] Wakeham, N., Bauer, E. D., Neupane, M. & Ronning, F. Large magnetoresistance in the antiferromagnetic semimetal NdSb. *Phys. Rev. B* 93, 205152 (2016).
- [35] Zeng, L.-K. et al. Compensated semimetal LaSb with unsaturated magnetoresistance. *Phys. Rev. Lett.* 117, 127204 (2016).

- [36] A. Vashist, R. K. Gopal, D. Srivastava, et al. Fermi surface topology and large magnetoresistance in the topological semimetal candidate PrBi. *Physical Review B* 99, 24, (2019) 245131.
- [37] Nayak, J., Wu, S., Kumar, N. et al. Multiple Dirac cones at the surface of the topological metal LaBi. *Nat Commun* 8, 13942 (2017)
- [38] Niu, X. et al. Presence of exotic electronic surface states in LaBi and LaSb. *Phys. Rev. B* 94, 165163 (2016).
- [39] Dey, Urmimala, et al. "Bulk band inversion and surface Dirac cones in LaSb and LaBi: Prediction of a new topological heterostructure. *Scientific reports* 8, 14867 (2018)
- [40] M. Ragragui, L. B. Drissi, E. H. Saidi, Evidence of topological surface states in dysprosium monpnictides compounds, *Materials Science & Engineering B* (2022)
- [41] Wu, Y. et al. Electronic structure of RSb (R = Y, Ce, Gd, Dy, Ho, Tm, Lu) studied by angle-resolved photoemission spectroscopy. *Phys. Rev. B* 96, 035134 (2017).
- [42] J. He, C.-F. Zhang, N. J. Ghimire, T. Liang, et al., Distinct Electronic Structure for the Extreme Magnetoresistance in YSb, *Phys. Rev. Lett.* 117, 267201 (2016).
- [43] Oinuma, H. et al. Three-dimensional band structure of LaSb and CeSb: absence of band inversion. *Phys. Rev. B* 96, 041120 (2017).
- [44] Kuroda, K. et al. Experimental determination of the topological phase diagram in cerium monpnictides. *Phys. Rev. Lett.* 120, 086402 (2018).
- [45] Li, P. et al. Tunable electronic structure and surface states in rare-earth monobismuthides with partially filled f shell. *Phys. Rev. B* 98, 085103 (2018).
- [46] P. Hohenberg and W. Kohn. Density functional theory (DFT). *Phys. Rev.* 136, B864 (1964).
- [47] W. Kohn and L. J. Sham. Self-consistent equations including exchange and correlation effects. *Phys. Rev.* 140, A1133 (1965).
- [48] Marzari N and Vanderbilt D. Maximally localized generalized Wannier functions for composite energy bands. *Phys. Rev. B* 56 12847 (1997)
- [49] Souza I, Marzari N and Vanderbilt D. Maximally localized Wannier functions for entangled energy bands. *Phys. Rev. B* 65 035109 (2001).
- [50] A. A. Mostofi, J. R. Yates, G. Pizzi, Y.-S. Lee, I. Souza, D. Vanderbilt, and N. Marzari. An updated version of wannier90: A tool for obtaining maximally-localised Wannier functions. *Comput. Phys. Commun.* 185, 2309 (2014).
- [51] Q. Wu, S. Zhang, H.F. Song, M. Troyer, and A. A. Soluyanov. WannierTools: An open-source software

package for novel topological materials. *Comput. Phys. Commun.* 224, 405 (2018).

[52] A. Vashist, et al., Fermi surface topology and large magnetoresistance in the candidate PrBi, *Physical Review B* 99.24 (2019) 245131.

[53] Liu, Z. et al. Observation of unusual topological surface states in half-Heusler compounds LnPtBi (Ln=Lu, Y). *Nat. Commun.* 7, 12924 (2016).